


# Narrow-band photon pair generation through cavity-enhanced spontaneous parametric down-conversion

Amideddin Mataji-Kojouri and Marco Liscidini *Dipartimento di Fisica, Università di Pavia, Via Agostino Bassi 6, 27100 Pavia, Italy*

(Received 27 June 2023; accepted 18 October 2023; published 20 November 2023)

Cavity-enhanced spontaneous parametric down-conversion (SPDC) can be used to implement heralded single-photon sources with narrow bandwidth down to tens of megahertz, thus compatible with atom-based quantum memories. In this work, we propose and study the cavities that are either singly resonant at the frequency of only one of the generated photons or doubly resonant at the frequency of one generated photon and for the pump field. We derive analytical expressions for the generation rate and the spectral brightness as a function of the main structure parameters. Our analysis shows that by exploiting counterpropagating SPDC inside a cavity with properly designed distributed Bragg reflectors, pure narrow-band heralded single photons can be generated. In particular, when a pulsed pump illuminates a 1-mm-long singly resonant cavity, the bandwidth of the resonant and the nonresonant photons will be 120 MHz and 5.7 GHz, respectively, with heralded single-photon purity as high as 0.993. Due to its small absorption probability inside the cavity, the heralding efficiency can approach unity if the nonresonant partner is used as a heralded single photon. Finally, we also show that continuous-wave excitation of a 1-cm-long cavity resonant for the pump and copropagating fields can provide photon pairs in a narrow bandwidth of 10 MHz with spectral brightness as high as  $2 \times 10^6$  (s mW MHz) $^{-1}$ . This source can efficiently couple with quantum memories and can find applications in quantum information processing and communication.

DOI: [10.1103/PhysRevA.108.053714](https://doi.org/10.1103/PhysRevA.108.053714)

## I. INTRODUCTION

In recent years, photonic quantum computing and quantum communication systems have grown more complex, and there has been a pressing demand for miniaturized and robust quantum photonic devices [1,2]. Generating nonclassical states of light is a cornerstone of quantum information processing [3]. Photon pair generation through spontaneous parametric down-conversion (SPDC) in nonlinear crystals is extensively employed in different quantum technologies [4]. In bulk crystals, photon pair generation rates can easily exceed 1 MHz/mW [5], and these sources are spectrally broad (e.g., bandwidths more than a few hundred GHz) [6]. For some specific applications, such as interfacing with quantum memories based on atomic transitions, narrow-band photon pairs are preferred. Indeed, quantum memories usually have an extremely narrow bandwidth associated with an atomic transition (e.g., about 100 MHz) [7]. Narrow-band photons are also desirable in experiments where one intends to perform characterizations in the time domain. Finally, narrow-band photons can also be exploited for generating time-bin-entangled photons [8]. Although it is possible to filter the bandwidth of generated photons, this comes at the cost of reduced efficiency.

An alternative approach makes use of cavity-enhanced SPDC [5,9–12]. In this connection, a theoretical study investigates sources with increased brightness using either doubly resonant cavities (where signal and idler frequencies are reso-

nant) or triply resonant cavities (where all fields involved in the nonlinear interaction are resonant) and a bright single-mode source is proposed based on passive filtering of the generated photons [10]. In another study, photon-pair generation through type-II SPDC in a singly-resonant cavity (resonant for the signal field and nonresonant for the idler field) is investigated [12,13]. Other works are focused on decreasing the bandwidth of photon pair generation through a doubly resonant cavity for the generated photon pairs [5]. In such a double-resonant configuration, different free spectral ranges (FSR) of the cavity resonances for the signal and idler fields give rise to the so-called clustering effect, in which only a small number of modes are doubly resonant. Thus, one can eventually achieve a single-longitudinal-mode emission with generation bandwidth compatible with quantum memories even without any additional filtering [11,14]. In these cases, one typically works with type-II SPDC to obtain substantially different FSRs for the signal and the idler fields, thereby leading to significantly smaller effective nonlinearity in most crystals [e.g., potassium titanyl phosphate (KTP) and lithium niobate]. Furthermore, achieving single-mode photon generation requires very high-quality factors that are obtained by working at critical coupling or under coupling conditions, which are characterized by low heralding efficiencies [14].

Another approach to narrow-band photon pair generation in quadratic nonlinear crystals is based on the interaction of counterpropagating fields where the partners propagate in reverse directions [15]. It is shown that heralded single photons with high purity can be generated in such a configuration [16,17]. The bandwidth of counterpropagating

\*marco.liscidini@unipv.it

photon-pairs is typically 2 orders of magnitude smaller than that of copropagating photon pairs [18]. A quasi-phase-matching condition for counterpropagating signal and idler waves usually requires submicron poling periodicity [19]. Poling crystals with such a small periodicity was not easily attainable until recently. There is a new report showing that by using a femtosecond laser nanodomains can be written in lithium niobate with very tiny feature sizes down to 30 nm [20]. Alternatively, it is possible to compromise on the generation rate by poling with an odd multiple of the submicron periodicity and satisfy a higher-order phase-matching condition. This approach has recently been implemented on a periodically poled KTP crystal [21] where the bandwidth of the backward-propagating photons was 7.43 GHz and the forward-propagating partner had a broad bandwidth of 230 GHz similar to that of the pump pulse. Although the bandwidth of the backward-propagating photons was reduced substantially, it was still about 2 orders of magnitude larger than that of typical atomic transitions.

In this paper, we focus on addressing the limitations of the aforementioned approaches. Most importantly, in order to increase the extraction efficiency of the generated photons, we employ a cavity which is resonant for the signal field and nonresonant for the idler. This configuration is, in principle, similar to the pioneering work of Herzog *et al.* [13] where the partners have orthogonal polarization and a polarizing beam splitter is used to deflect the idler photons out of the cavity, so that the cavity is only resonant for the signal and pump fields. Here, we employ frequency-selective dielectric Bragg reflectors to implement a singly-resonant cavity for photon pairs that are with the same polarization but are different in frequency. This allows us to exploit the strong type-0 nonlinear interaction where all involved fields have the same polarization. In this configuration, generated single photons display a bandwidth in the tens of megahertz up to gigahertz range which is controllable by the linewidth of the signal resonance. Since the cavity is nonresonant for the idler field, the source will produce a high-dimensional biphoton frequency comb once the substrate is periodically poled for copropagating partners as the phase-matching bandwidth will be too broad [22]. Here, we show that single-mode emission is also achievable in such a singly-resonant cavity if we use a substrate that is poled for counterpropagating partners. In our analysis, we consider a process which is highly non-degenerate with a pump field at 532 nm, the signal field at around 890 nm compatible with Nd-based atomic quantum memories [14], and the idler field at around 1320 nm. By taking realistic parameters into account, we show that cavity-enhanced SPDC for counterpropagating partners enables efficient single-longitudinal-mode narrow-band photon pair generation with high extraction efficiency. The proposed structure is based on a monolithic periodically poled lithium niobate substrate with dielectric mirrors deposited on its end facets. In our proposal, the pump field can be resonant in addition to the resonance for the signal field in order to increase the brightness of the source. The heralding efficiency of this source can approach unity because the cavity is nonresonant for the idler photon and the probability of its absorption is thus negligible. Consequently, detection of the herald signal photon assures the presence of the heralded idler photon out

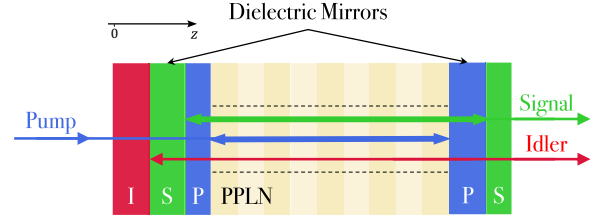


FIG. 1. A monolithic photon-pair source based on cavity-enhanced SPDC. The cavity is formed by depositing dielectric mirrors at the end facets of a periodically poled LiNbO<sub>3</sub> substrate. A hypothetical waveguide region is shown by dashed lines. The cavity is resonant for pump and signal fields and there is an additional dielectric mirror for the idler field on the left side to ensure idler photons exit only from the right side. Mirrors are designed so that the pump field is critically coupled on the left side and the signal field is so on the right side. Other mirrors are highly reflective to eliminate unwanted scattering losses.

of the cavity. If the poling periodicity satisfies the quasi-phase-matching condition for copropagating waves, the output will be a multimode frequency bin suitable for parallel quantum computing and communication schemes [22]. For a substrate that is quasi-phase-matched for counterpropagating signal and idler fields, a singly resonant configuration enables single-mode emission of photons with controllable bandwidths in a range from as narrow as tens of megahertz up to gigahertz under both cw and pulsed excitation. In the case of pulsed excitation, factorizable biphoton joint spectral amplitude (JSA) is achievable with the purity of the heralded single photons arbitrarily close to unity.

The structure of the paper is as follows. In Sec. II, we present the structure under consideration and the strategy adopted to achieve singly resonant and doubly resonant conditions. In Sec. III, we investigate the state of the generated photon pairs. In the case of cw pumping, we derive analytical expressions for the generation rate and the spectral brightness of the source and validate their predictions with those from numerical simulations. In the case of pulsed excitation, we study frequency correlations and factorizability of the state. In Sec. IV we compare our results in terms of brightness, heralding efficiency, number of cavity modes, and other properties of the source with those reported in the literature on cavity-enhanced SPDC LiNbO<sub>3</sub> sources. Finally in Sec. V we draw our conclusions.

## II. LINEAR RESPONSE OF THE MONOLITHIC CAVITY

Figure 1 shows a schematic of a cavity-enhanced SPDC source composed of a LiNbO<sub>3</sub> crystal sandwiched between two dielectric mirrors. We consider a pump field (either pulsed or quasi-cw) operating at a central wavelength of 532 nm, with the signal and idler wavelengths around 895 and 1320 nm, respectively. The mirrors are composed of different parts that are specifically designed to optimize the overall response in these three wavelength ranges. At the pump frequency, the mirror on the right side is highly reflective, and the mirror on the left side is tailored to satisfy the critical coupling condition to achieve the strongest field enhancement. In the signal (S) frequency range, the resonator is designed to be in

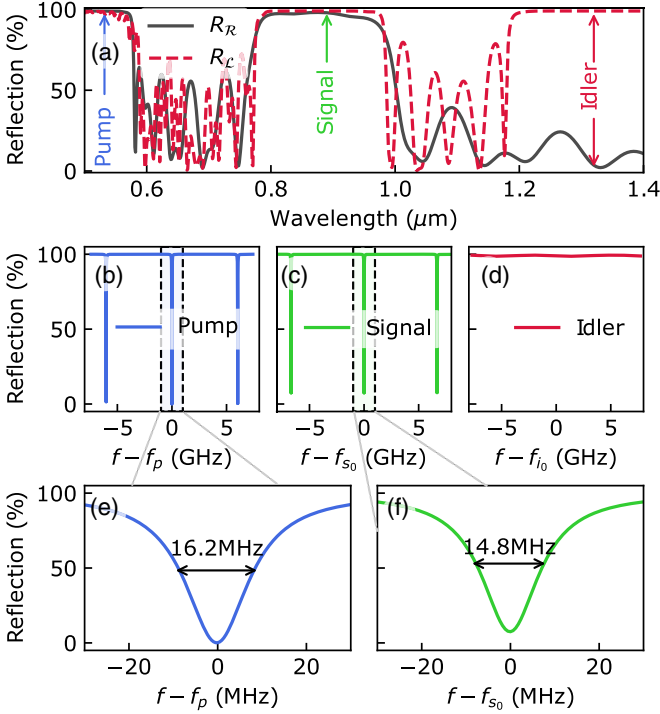


FIG. 2. (a) Reflection spectra of the right ( $R_R$ ) and left ( $R_L$ ) dielectric mirrors. The left mirror is designed to critically couple the pump field but totally reflect the signal field. On the contrary, the right mirror has a very high reflectivity at the pump frequency and critically couples the signal field to the output. Reflection from the cavity near the pump (incident from left) (b), signal (incident from right) (c), and idler (incident from right) (d) frequencies. No resonances are visible in the reflection spectrum around the idler frequency. Magnified view of the reflection spectra at pump (e) and signal (f) frequencies.

the overcoupling regime, with the right mirror having nearly unity reflectivity to ensure signal emission only on the right side. Finally, only the right mirror is highly reflective in the idler (I) frequency range, so the system is not resonant in this frequency range. This ensures that the collection efficiency of the idler photons is nearly unity, limited only by a small amount of absorption or scattering losses within the LiNbO<sub>3</sub> crystal. We assume that the fields in the nonlinear crystal are gently confined in the transverse direction, either by implementing an ion-diffusion waveguide (shown with dashed lines in the schematic). Alternatively, one can envision curved highly reflective metallic coating on one side of the crystal [8,23] and deposit Bragg reflectors on the other side to laterally confine the modes. For the design of the mirrors, we consider quarter-wavelength layers composed of alternating TiO<sub>2</sub> and SiO<sub>2</sub> thin films. In our calculations we include the material chromatic dispersion by using measured values of the refractive indexes of LiNbO<sub>3</sub>, TiO<sub>2</sub>, and SiO<sub>2</sub> layers [24–27]. In accordance with recent experiments on LiNbO<sub>3</sub>, we assume that the linear loss in the nonlinear crystal at all involved frequencies is some 0.02 dB/cm [14].

Figure 2(a) shows the reflection spectra of the right  $R_R$  and left  $R_L$  mirrors. The left mirror stack is composed of 15 bilayers for the signal frequency, 15 bilayers for the idler

frequency, and 8 bilayers for the pump frequency. As a result, the pump field is critically coupled, and the signal and idler fields are totally reflected. On the right side, the mirror is made of 9 bilayers for the signal field and 15 bilayers for the pump field. Figures 2(b)–2(f) show the corresponding reflection spectra of the entire system in the different frequency ranges. Specifically, Fig. 2(b) shows the reflection spectrum for the pump incident from the left side of the structure. Three resonances of the cavity are shown: the resonance width for the pump resonance is about 16.2 MHz [Fig. 2(e)], and the free spectral range (FSR) is about 6 GHz. In Fig. 2(c) we show the reflection spectrum for the signal for an excitation from the right side. The signal resonance width is 14.8 MHz as shown in Fig. 2(f), with an FSR of about 6 GHz. Finally, in Fig. 2(d) we show the reflection spectrum at the idler frequency, which confirms that the cavity is nonresonant in this frequency range.

### III. CHARACTERIZATION OF THE PHOTON PAIR SOURCE

We now turn to the problem of calculating the state of the generated pairs in this structure. If the probability of generating a photon pair per pump pulse is sufficiently small, the state for the generated photon pairs can be written as [28]

$$|II\rangle = \frac{1}{\sqrt{2}} \int d\omega_1 d\omega_2 \phi(\omega_1, \omega_2) a_{\omega_1}^\dagger a_{\omega_2}^\dagger |\text{vac}\rangle. \quad (1)$$

Here  $a_{\omega_i}^\dagger$  is the creation operator for the photon at  $\omega_i$ , and

$$\phi(\omega_1, \omega_2) = i \frac{\alpha \bar{\chi}_2}{\beta} \sqrt{\frac{\hbar \omega_1 \omega_2 (\omega_1 + \omega_2)}{8\pi \epsilon_0 n_{\omega_1} n_{\omega_2} n_{\omega_1 + \omega_2} c^3 \mathcal{A}}} \times \phi_P(\omega_1 + \omega_2) J(\omega_1, \omega_2, \omega_1 + \omega_2) \quad (2)$$

is the biphoton wave function.  $|\alpha|^2$  is the average number of photons per pump pulse,  $\bar{\chi}_2$  is a typical value of second-order nonlinearity,  $\mathcal{A}$  is the effective area,  $\omega_1$  and  $\omega_2$  are respectively the angular frequency of the first and the second photon,  $n_\omega$  is the effective index of the mode at corresponding frequency, and  $\phi_P(\omega)$  is the pump spectral profile [28].  $J$  is the field distribution integral for the case where the structure is pumped from the left and generated pairs exit from the right side and is defined as [29]

$$J(\omega_1, \omega_2, \omega_1 + \omega_2) = \int_0^L dz \frac{\chi_2^{ijk}(z)}{\bar{\chi}_2} f_{\mathcal{R}, \omega_1}^j(z) f_{\mathcal{R}, \omega_2}^k(z) f_{\mathcal{L}, \omega_1 + \omega_2}^i(z). \quad (3)$$

Here  $f_{\mathcal{L}(\mathcal{R}), \omega}^i(z)$  is the  $i$  component of the field enhancement corresponding to the solution of the linear Maxwell equations at the angular frequency  $\omega$  with field input from the left (right). Finally, the average number of photon pairs generated per pump pulse is given by [30]

$$|\beta|^2 = |\alpha|^2 \bar{\chi}_2^2 \frac{\hbar \omega_S \omega_I \omega_P}{8\pi \epsilon_0 n_S n_I n_P c^3 \mathcal{A}} \times \int d\omega_1 d\omega_2 |\phi_P(\omega_1 + \omega_2) J(\omega_1, \omega_2, \omega_1 + \omega_2)|^2, \quad (4)$$

which follows directly from the state normalization.

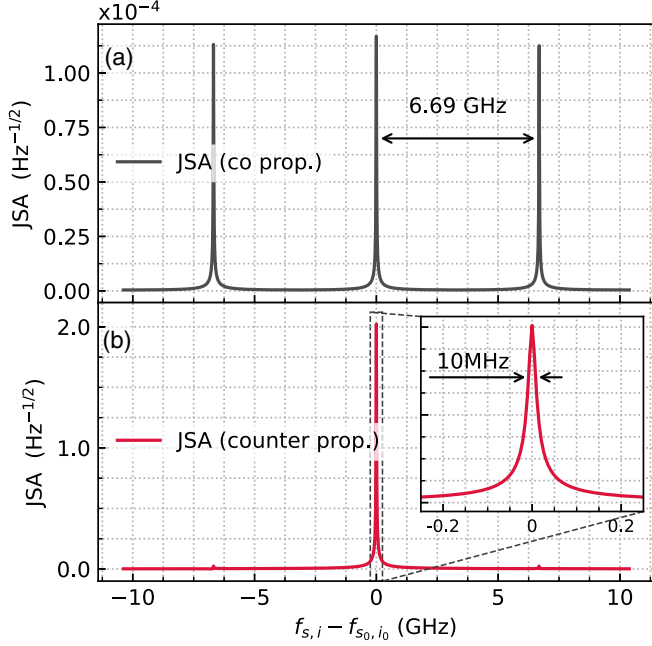


FIG. 3. Joint spectral amplitude calculated numerically for the mirror stacks with reflection spectra shown in Fig. 2, when the crystal is periodically poled for copropagating (a) and counterpropagating (b) idler fields. In the case of the copropagating idler field, the spectrum is comblike for both signal and idler frequency ranges despite the idler field being nonresonant. For the counterpropagating idler field, the spectrum displays only one resonance due to the narrow-band phase-matching condition.

#### A. Continuous-wave excitation

When the structure shown in Fig. 1 is excited by a very long pulse compared to the cavity lifetime, thus in the limit of a quasi-cw pump at  $\omega_P$ , the biphoton wave function can be written in terms of a single-variable function because of the energy conservation relation  $\omega_P = \omega_1 + \omega_2$ . One can calculate the biphoton wave function using two different approaches.

In the first one, we use a transfer matrix method (TMM) to calculate the asymptotic fields at pump, signal, and idler frequencies. The biphoton wave functions calculated for the copropagating phase matching and the counterpropagating phase matching are shown in Figs. 3(a) and 3(b), respectively. For the copropagating case, the structure generates a biphoton frequency comb over the phase-matching bandwidth [only three resonances are visible in Fig. 3(a)] with a frequency spacing equal to the FSR of the cavity at the signal frequency. Notably, although the system is not resonant at the idler frequencies, the spectrum of the idler photons is also comblike, due to the combination of energy conservation and signal resonant field enhancement. It can be shown that in our system the bandwidth of the phase-matching function for the counterpropagating case is narrower than twice the cavity FSR. Hence, for this case the biphoton wave function displays only *one* resonance. This is an important result because one can archive a single-resonant operation with a 10-MHz bandwidth.

In addition to this numerical study, the system is sufficiently simple to derive the expressions of the biphoton wave

function analytically with minimal approximations. This is particularly useful because one can also derive an analytic expression of the generation rate as a function of the most important source parameters. In this approach, one starts with Airy functions to describe the resonant fields inside the Fabry-Pérot resonator and neglects small reflections of the idler at the right end of the cavity. We refer to the Appendix for all the calculation details. The photon pair generation rate in the long-pulse limit and within one free spectral range of the cavity is

$$|\beta|^2 = |\alpha|^2 \bar{\chi}_2^2 \frac{4\hbar\omega_S\omega_I}{\pi^2\epsilon_0 n_S^3 n_I n_P^3 c \mathcal{A}} \frac{Q_P^2}{Q_{P,c}} \frac{Q_S}{Q_{S,c}}, \quad (5)$$

where  $Q_P$  and  $Q_S$  are the loaded quality factors of the pump and signal resonances, respectively. Similarly,  $Q_{P,c}$  and  $Q_{S,c}$  are the corresponding quality factors determined by the sole coupling due to the mirrors. For a cavity critically coupled at pump and signal frequencies ( $Q_{S,c} = 2Q_S$ ,  $Q_{P,c} = 2Q_P$ ), the generation rate expression simplifies to

$$|\beta|^2 = |\alpha|^2 \bar{\chi}_2^2 \frac{\hbar\omega_S\omega_I}{\pi^2\epsilon_0 n_S^3 n_I n_P^3 c \mathcal{A}} Q_P. \quad (6)$$

From these results, it appears that the generation rate is independent of the cavity length  $L$ . This is indeed the case in the absence of propagation losses and when only two of the fields involved in SPDC (in this case, the pump and signal) are resonantly enhanced. This curious result can be understood by considering that the generation rate scales quadratically with the length of the nonlinear material, while the intensity enhancement of each field is inversely proportional to the cavity length. Importantly, in the case of absorption or scattering inside the nonlinear material, the length of the cavity is implicitly contained in the loaded  $Q$  factors, as it has an impact on the quality factors of the involved resonances [please see Eq. (A8)]. For short crystals where the loss is negligible, the loaded quality factor is essentially the coupling quality factor, which increases linearly with length. On the contrary for longer cavities, when losses dominate, the loaded quality factor saturates to the intrinsic quality factor. Another interesting result is that in the absence of loss ( $Q_S = Q_{S,c}$ ,  $Q_P = Q_{P,c}$ ) or in a regime of strong overcoupling, Eq. (5) shows that the overall generation rate scales linearly with a quality factor of the cavity at pump frequency ( $Q_P$ ) and is independent of the signal quality factors. Yet, it should be noted that the bandwidth of the generated photons [Eq. (A7)] and hence the spectral brightness of the source ( $|\beta|^2/\Delta\omega$ ) [see also Eq. (A7)] still depend on the signal quality factor.

As an example, we study the photon pair generation rate for a cavity with length ( $L$ ) between 0.1 and 2 cm, effective area  $\mathcal{A} = 100 \mu\text{m}^2$ ,  $\bar{\chi}_2 = \chi_2^{zzz} = 54 \text{ pm/V}$  [31], and dielectric mirrors as described in Sec. II. Figure 4 shows the source generation rate and the brightness calculated numerically using TMM and analytically using Eq. (5). The results are in good agreement and show that there exist two optimal lengths, for which either the generation rate or the brightness is maximum. These results can be easily understood by looking at Eq. (5). Indeed, when the cavity is very short ( $L \ll (1 - |r|)/2\alpha_e$ ), coupling ( $Q_c$ ) and loaded ( $Q$ ) quality factors are almost equal due to the negligible loss inside the cavity, and thus



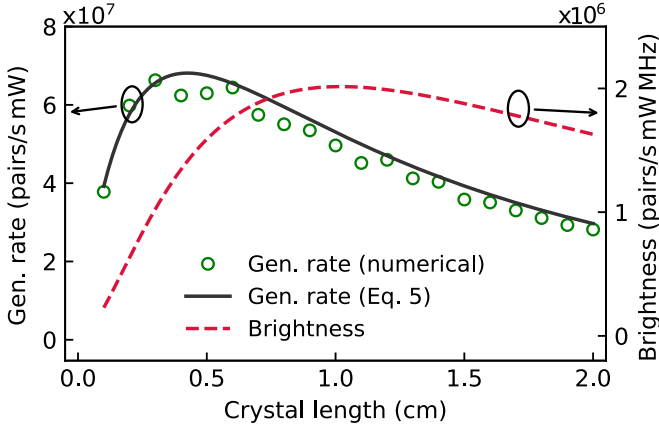


FIG. 4. Left axis: Photon-pair generation rate calculated numerically or using the analytical formula as provided in the text for a Fabry-Pérot cavity enclosing a LiNbO<sub>3</sub> crystal of length  $L$  between 0.1 and 2 cm formed by distributed Bragg reflector stacks with their respective reflectivity shown in Fig. 2(a). Right axis: Spectral brightness of the source predicted analytically.

both the rate and the brightness increase linearly with  $Q_P$ , which is proportional to  $L$ . By increasing the length further ( $L > (1 - |r|)/2\alpha_e$ ), the loss dominates the loaded quality factors which saturate, and thus the generation rate and the brightness are dominated by the increasing coupling quality factor. It should be noted that the maximum generation rate occurs when the resonator is slightly overcoupled [32].

### B. Pulsed excitation

We now consider the case in which the structure of Fig. 1 is excited by a pulse. This is an interesting case, because pulse excitation is necessary to generate photon pairs in a separable state (in a single Schmidt mode) to implement heralded single-photon sources. As shown in the Appendix, the spectral properties and the brightness of the source depend on three important elements: the phase-matching factor along the nonlinear crystal, the field enhancement at the resonant frequency, and the spectral shape of the pump pulse, which controls energy conservation. In this work, we consider the most common case of a Gaussian pulse defined by

$$\phi_P(\omega) = \left( \sqrt{\frac{\pi}{2}} \Delta\Omega \right)^{-1/2} e^{-[(\omega - \omega_P)/\Delta\Omega]^2}, \quad (7)$$

with  $\omega_P$  being the center angular frequency of the pulse and  $\Delta\Omega$  being its bandwidth.

In Fig. 5(a), we illustrate the most important factors that are involved in determining the final form of the JSA for our system in the case of a LiNbO<sub>3</sub> crystal of length  $L = 1$  mm that is quasi-phase-matched for counterpropagating idler and signal fields. We used measured values for the frequency-dependent refractive indexes of LiNbO<sub>3</sub> using the values reported in Ref. [25]. In this case, the phase matching is satisfied in the spectral interval indicated in green, which is characterized by a very narrow bandwidth (about 100 GHz) for the idler and a relatively wide one (several FSRs) for the signal photon. Vertical bands of width  $\delta f_S$  account for the

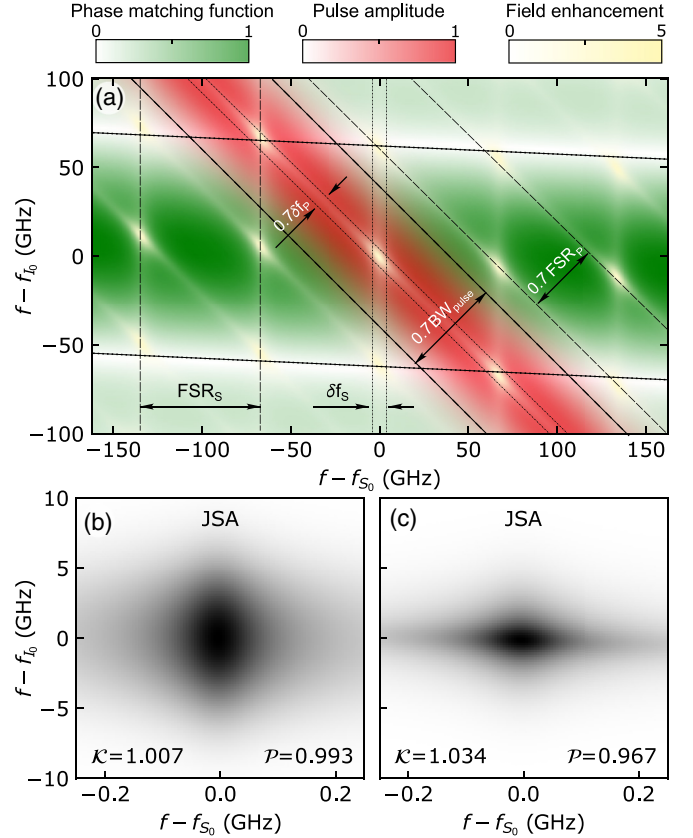


FIG. 5. (a) Superimposed surface plots as functions of signal and idler photon frequencies showing the phase-matching function (green color map), the pulse amplitude (red color map), and the field amplitude enhancement (yellow color map) for a crystal length of  $L = 1$  mm. For this graph, a relatively small mirror reflectivity ( $|r_{L,\omega_P}|^2 = |r_{R,\omega_S}|^2 = 0.4$ ) is used for better visibility. Factorizable JSA with purity near unity for a pump pulse with  $\tau_d = 200$  ps when the pump field is either nonresonant (b) or resonant (c). The bandwidth of the signal photon can be directly controlled by the reflectivity of the mirror at the signal frequency. As for the idler, the photon bandwidth can be controlled to a degree by the cavity for the pump field and the state remains factorizable if  $\Delta\omega_P \ll \Delta\omega_S$ .

signal field enhancement, and the antidiagonal bands of width  $\delta f_S$  describe the field enhancement associated with the pump resonances. Finally, the pulse spectral width is represented by an antidiagonal red strip, which indicates the spectral region in which energy conservation can be satisfied. Naturally, photon pairs are generated mostly when all the conditions (i.e., phase matching, field enhancement, and energy conservation) are simultaneously satisfied, which is in the narrow region at the center of the figure in which all the areas overlap.

While the phase-matching condition and the resonant field enhancement are determined by the structure, as usual one can control the spectral correlations of the generated photons by playing with the pump properties. In Fig. 5, by exciting the system with a pulse having a bandwidth smaller than the pump FSR but larger than the line width of the pump resonance, it is possible to achieve single-mode operation with photon pairs generated in a nearly separable state. As a first example, in Fig. 5(b), we show the biphoton wave function

TABLE I. Overview of recent cavity-enhanced SPDC sources in LiNbO<sub>3</sub>.

Metric	[33]	[14]	[34]	This work <sup>a</sup>	
Crystal length (mm)	6	12.3	20	10	1
Bandwidth (MHz)	48	66	3	10	120, 5700
Wavelengths (nm)	532; 890+1320	532; 890+1320	426; 606+1436	532; 890+1320	
SR/DR/filter <sup>b</sup>	SR (S)+filter	DR (S,I)	DR (S,I)+filter	DR (P,S)	SR (S)
Number of cavity modes	8-9 modes	Single mode	Single mode	Single mode	
Excitation	cw	cw	cw	cw	Pulsed
Brightness (s mW MHz) <sup>-1</sup>	5 <sup>c</sup>	3 × 10 <sup>4d</sup>	2.2 × 10 <sup>3d</sup>	2 × 10 <sup>6</sup>	—
Heralding efficiency (%)	10.3	18 (28) <sup>e</sup>	28	<98 <sup>f</sup>	<99 <sup>f</sup>

<sup>a</sup>In contrast to other results summarized in the table, this column is based on simulations. We assumed an effective area of  $\mathcal{A} = 100 \mu\text{m}^2$ .

<sup>b</sup>SR, singly-resonant cavity; DR, doubly-resonant cavity; P, pump; S, signal; I, idler.

<sup>c</sup>Measured brightness at the detector without correcting for the loss.

<sup>d</sup>Inferred brightness of the source corrected for losses.

<sup>e</sup>Based on reported escape probabilities of signal and idler photons which are 28% and 18%, respectively.

<sup>f</sup>Considering material absorption and mirror reflectivities (without accounting for possible transmission losses between the cavity output and the detector).

for a cavity which is only resonant for the signal, where we considered the signal mirror reflectivity  $|r_{\mathcal{R},\omega_s}|^2 = 0.99$ . We employed the Schmidt decomposition of the generated biphoton state to characterize its factorizability. Here the heralded single-photon purity is equal to the reciprocal of the Schmidt number of the corresponding two-photon state (herald plus heralded) [35]. The calculated Schmidt number for the two-photon state is  $\mathcal{K} = 1.007$ , which corresponds to a heralded photon purity of  $\mathcal{P} = 0.993$ . In this case, the signal photons have a bandwidth of about 120 MHz, and the idler photon bandwidth is about 5.7 GHz. As a second example, we study the case of a cavity that is also resonant with the pump. The result is shown in Fig. 5(b), where we consider the pump mirror reflectivity  $|r_{\mathcal{L},\omega_p}|^2 = 0.8$ . In this case, signal and idler photon bandwidths are 115 MHz and 2.1 GHz, respectively. Since the bandwidth of the pump resonance is much larger than that of the signal resonance, the two-photon state is still nearly separable. The Schmidt number  $\mathcal{K} = 1.034$ , which corresponds to a single-photon purity of  $\mathcal{P} = 0.967$ . These two examples show the flexibility and the tunability of this cavity system.

#### IV. DISCUSSION AND COMPARISON

We can compare the system analyzed in the previous section with some of the most relevant works on cavity-enhanced LiNbO<sub>3</sub> SPDC sources in which the cavity is either singly resonant or doubly resonant. It should be noticed that this comparison is not aimed at identifying the optimal structure for a given application, but we rather want to highlight what are the differences and similarities with previous studies in which only a part of the fields involved in the nonlinear interaction is resonantly enhanced. Our comparison is summarized in Table I, in which we consider crystal length, emission bandwidth, operational wavelength range, number of cavity modes, type of excitation, spectral brightness, and heralding efficiency. The features of our structures are contained in the last two columns for the singly resonant and doubly resonant cases.

The main difference between previous work is that in our systems we can generate photons in a single-longitudinal

mode of the cavity without any predetection filtering even when the cavity is only resonant for the signal field. Indeed, in Ref. [33], filtering is employed to select eight or nine modes of the generated biphoton frequency comb. The selection of a single longitudinal mode in doubly resonant cavities may [34] or may not [14] need additional filtering depending mostly on the type of the phase-matching condition. In our structure, we predict a very high brightness of about  $2 \times 10^6$  (s mW MHz)<sup>-1</sup> for a doubly resonant system. Interestingly, this is significantly larger than what was reported for previous work even if the idler field is not resonant with the cavity. A higher brightness means that the photon pair generation process has become more efficient, and the amount of the required input pump power is reduced. Hence, the increase in brightness does not degrade the quality of the source as long as one can keep the absolute generation rate low enough to avoid significant multiple-pair generation [36,37].

In contrast to the previous works shown in the table, the proposed configuration can be excited with a pulsed pump and generate factorizable biphoton states. Our calculations show that for a crystal with a length of 1 mm and pulse duration as short as 200 ps, one can achieve a factorizable biphoton state with signal photons having a bandwidth of 120 MHz and idler photons having a bandwidth of about 5.7 GHz. Interestingly, the heralding efficiency, which is the probability of a heralded photon exiting the cavity knowing that the herald photon is detected, exceeds that of DR sources where both idler and signal fields are resonant. Indeed, since the idler field is not resonant, if one uses the signal photon as the herald, the heralding efficiency can approach unity, limited only by the intrinsic loss inside the cavity. In the heralding efficiency calculation, the reflectivities of the mirrors for the idler field are taken from Fig. 2(a) where  $|r_{\mathcal{L}}|^2 \approx 0.99$ ,  $|r_{\mathcal{R}}|^2 \approx 0.031$  and the crystal loss is 0.02 dB/cm. Here we do not take into account transmission losses from the cavity output to the detectors.

#### V. CONCLUSIONS

In summary, this study explores a heralded single-photon source that utilizes cavity-enhanced spontaneous parametric down-conversion (SPDC) in a periodically poled lithium

niobate nonlinear crystal for contrapropagating phase matching. The distinctive characteristic of the proposed devices is that it is resonant for both the pump and the signal fields, but nonresonant for the idler field. This configuration facilitates lossless extraction of idler photons and potentially allows for nearly perfect heralding efficiency when using the signal photon as a herald. Moreover, despite the nonresonant nature of the idler field, the source remains single-mode without necessitating any predetection filtering. This is attributed to the narrow phase-matching condition inherent in the counterpropagating interaction. Our analysis reveals that, even without optimization of the crystal length or mirror reflectivity, the brightness of our proposed source can surpass that of doubly resonant sources that are resonant with the idler and signal photons by 2 orders of magnitude. This result is attributed to five key factors: (i) the use of type-0 nonlinear interaction, which yields a nonlinear coefficient nearly an order of magnitude greater than type-I or type-II interactions that are predominantly used in sources based on the clustering effect; (ii) the implementation of a highly reflective mirror on one side of the cavity, ensuring that generated photon pairs can only exit through the output side; (iii) virtually no loss of idler photons in the cavity due to the nonresonant configuration, resulting in pair extraction efficiency that is primarily limited by the resonant absorption of signal photons; (iv) since the source is not based on clustering effect, one can operate in an over coupled coupling region for the signal resonance, reducing resonant absorption; and (v) the cavity's resonance with the pump field enhances the field at the pump, boosting brightness without negatively impacting other source attributes under continuous-wave excitation. Additionally, a standout feature of our source is its compatibility with pulsed excitation as an alternative to continuous-wave lasers, while still maintaining single-mode emission. As far as we are aware, this flexibility has not been realized in narrow-band sources reliant on clustering effects. Our findings demonstrate that the biphoton state of the pairs generated under pulsed excitation is factorizable, and the purity for a heralded single-photon source employing this configuration can be as high as 0.993, as calculated through Schmidt decomposition. Furthermore, we establish that by tuning the mirror reflectivity, it is possible to control the bandwidth of both idler and signal photons without compromising purity or pair generation rates. Additionally, the idler photon bandwidth can be modulated by adjusting the duration of the excitation pulse.

Finally, the findings from this research extend beyond the specific devices under consideration; indeed the expression for the generation rate and the spectral brightness reported in this work holds also for other doubly resonant sources as well. They serve to highlight the essential factors to be taken into account when designing sources using SPDC. Thus, the implications of this research are important for a broader scope of applications in the generation of nonclassical light.

#### ACKNOWLEDGMENT

We acknowledge support by PNRR MUR Project No. PE0000023-NQSTI.

#### APPENDIX

To estimate the overlap integral, we consider the high reflectivity of the right dielectric mirror for the pump and the left dielectric mirrors for the idler and signal fields and we neglect the impact of the attenuation constant on the amplitude of the forward and backward propagating waves. In this case, the field distribution for our configuration for excitation from left (for the pump field) or right (for the signal and idler fields) can be written respectively as

$$\begin{aligned} f_{\mathcal{L},\omega}(z) &\approx E_{\omega}(e^{-jk_{\omega}z} + e^{+jk_{\omega}z+j\delta_{\omega}}) \quad \text{and} \\ f_{\mathcal{R},\omega}(z) &\approx E_{\omega}(e^{-jk_{\omega}z+j\delta_{\omega}} + e^{+jk_{\omega}z}), \end{aligned} \quad (\text{A1})$$

where  $k_{\omega}$  is the propagation constant in the crystal at the frequency  $\omega$ .  $\delta_{\omega} = -k_{\omega}L - \theta_{\omega}$  is the phase difference between incident and reflected waves inside the cavity at the corresponding frequency, where  $\theta_{\omega}$  is the reflection phase of the Bragg mirror,  $E_{\omega}$  is the electric field enhancement inside the cavity, and  $L$  is the length of the resonator. We assume that the substrate is periodically poled for type-0 copropagating quasi-phase matching at pump, signal, and idler frequencies so that the poling wave vector satisfies  $k_{pp} = k_P - k_S - k_I$ . At other frequencies, we define  $\Delta k(\omega_1, \omega_2, \omega_3 = \omega_1 + \omega_2) = k_{\omega_3} - k_{\omega_1} - k_{\omega_2} - k_{pp}$ . Hence, after dropping superscripts for components of the fields and the nonlinearity tensor, and defining  $k_i = k_{\omega_i}$ , the field distribution integral defined in Eq. (3) simplifies to

$$\begin{aligned} J(\omega_1, \omega_2, \omega_3) &= \int_0^L dz \frac{\chi_2(z)}{\bar{\chi}_2} f_{\mathcal{R},\omega_1}(z) f_{\mathcal{R},\omega_2}(z) f_{\mathcal{L},\omega_3}(z) \\ &= E_{\omega_1} E_{\omega_2} E_{\omega_3} \int_0^L dz \frac{2}{\pi} (e^{-jk_{pp}z} + e^{+jk_{pp}z}) \\ &\quad \times (e^{-jk_1z+j\delta_1} + e^{+jk_1z}) \times (e^{-jk_2z+j\delta_2} + e^{+jk_2z}) \\ &\quad \times (e^{-jk_3z} + e^{+jk_3z+j\delta_3}) \\ &= \frac{4L}{\pi} E_{\omega_1} E_{\omega_2} E_{\omega_3} \text{sinc}(\Delta kL/2) e^{j\delta_f/2} \\ &\quad \times \cos[(2k_1 + 2k_2 + k_{pp})L/2 + \theta_0], \end{aligned} \quad (\text{A2})$$

where  $\delta_f = \delta_1 + \delta_2 + \delta_3$ , and in the first equation we replaced the periodic nonlinearity profile  $\chi_2(z)/\bar{\chi}_2$  with the first two terms of its Fourier expansion. Similarly, for a substrate that is quasi-phase-matched for a counterpropagating idler field, that is, the wave vectors satisfy  $k_{pp} = k_P - k_S + k_I$  and  $\Delta k = k_{\omega_3} - k_{\omega_1} + k_{\omega_2} - k_{pp}$ , the field distribution integral is

$$\begin{aligned} J(\omega_1, \omega_2, \omega_3) &= \frac{4L}{\pi} E_{\omega_1} E_{\omega_2} E_{\omega_3} \text{sinc}(\Delta kL/2) e^{j\delta_f/2} \\ &\quad \times \cos[(2k_1 - 2k_2 + k_{pp})L/2 + \theta'_0]. \end{aligned} \quad (\text{A3})$$

In our analysis, for the case of continuous-wave excitation of the system, we neglect the impact of the cosine factor as it can be largely compensated by tailoring the crystal length or slight temperature variations in an experiment. The intensity ( $I = |E|^2$ ) enhancement for a lossy Fabry-Pérot resonator containing a crystal with the refractive index  $n$ , the field absorption coefficient  $\alpha_E$ , and mirror reflectivities  $r_{\mathcal{L}}$  and  $r_{\mathcal{R}}$ , respectively, for its left and right mirrors, when excited by an

incident wave from the left side, is given by [38]

$$\frac{I_{\text{FP}}}{I_{\text{inc}}} = \frac{(1 - |r_{\mathcal{L}}|^2)/n}{(1 - |r_{\mathcal{L}}r_{\mathcal{R}}|e^{-2\alpha_E L})^2 + 4|r_{\mathcal{L}}r_{\mathcal{R}}|e^{-2\alpha_E L} \sin^2 \phi}, \quad (\text{A4})$$

with  $\phi = k_{\omega}L$ . The enhancement factor for a Fabry-Pérot resonance integrated over one free spectral range is [38]

$$\int d\omega \frac{I_{\text{FP}}}{I_{\text{inc}}} = \frac{\pi c}{Ln_{\omega}} \frac{(1 - |r_{\mathcal{L}}|^2)/n}{1 - |r_{\mathcal{L}}r_{\mathcal{R}}|^2 e^{-4\alpha_E L}}, \quad (\text{A5})$$

with  $c$  being the speed of light in *vacuo* and  $n_{\omega}$  being the refractive index of the crystal. By substituting these results in Eq. (4), the generation rate can be calculated from

$$\frac{|\beta|^2}{|\alpha|^2} = \bar{\chi}^2 \frac{2\hbar\omega_I\omega_S\omega_P L}{\pi^2 \varepsilon_0 n_I n_S^3 n_P^2 c^2 \mathcal{A}} \frac{1 - |r_{\mathcal{L},\omega_P}|^2}{(1 - a_{rt}^2)^2} \frac{1 - |r_{\mathcal{R},\omega_S}|^2}{1 - a_{rt}^4}, \quad (\text{A6})$$

where  $a_{rt}^2 = |r_{\mathcal{L}}r_{\mathcal{R}}|e^{-2\alpha_E L}$  is the round-trip loss factor. Considering the asymmetric mirror design described in the text,

the round-trip loss factor reduces to  $a_{rt}^2 = |r_{\mathcal{L},P}|e^{-2\alpha_E L}$ , and  $a_{rt}^2 = |r_{\mathcal{R},S}|e^{-2\alpha_E L}$  for pump and signal fields, respectively. Equation (A4) can be used to calculate the full width at half maximum of the resonance

$$\Delta\omega = 2 \arcsin \frac{1 - |r_{\mathcal{L}}r_{\mathcal{R}}|e^{-2\alpha_E L}}{2\sqrt{|r_{\mathcal{L}}r_{\mathcal{R}}|e^{-2\alpha_E L}}} \frac{c}{Ln}, \quad (\text{A7})$$

with  $n$  being refractive index of the crystal. Hence, the loaded quality factor of the resonance is

$$Q \approx \frac{\omega Ln}{c} \frac{a_{rt}}{1 - a_{rt}^2}. \quad (\text{A8})$$

The coupling quality factor ( $Q_c$ ) is calculated from Eq. (A8) by eliminating the impact of intrinsic loss inside the resonator (e.g., by setting  $a_{rt}^2 = |r_{\mathcal{L}}r_{\mathcal{R}}|$ ). One can rewrite Eq. (A6) in terms of the quality factors of the resonances involved in the process to obtain Eq. (5).

- 
- [1] S. Slussarenko and G. J. Pryde, *Appl. Phys. Rev.* **6**, 041303 (2019).
  - [2] J. Wang, F. Sciarrino, A. Laing, and M. G. Thompson, *Nat. Photon.* **14**, 273 (2020).
  - [3] D. V. Strekalov and G. Leuchs, in *Quantum Photonics: Pioneering Advances and Emerging Applications*, edited by R. W. Boyd, S. G. Lukishova, and V. N. Zadkov (Springer, Berlin, 2019), Chap. 10, pp. 51–100.
  - [4] C. Couteau, *Contemp. Phys.* **59**, 291 (2018).
  - [5] O. Slattery, L. Ma, K. Zong, and X. Tang, *J. Res. Natl. Inst. Stand. Technol.* **124**, 124019 (2019).
  - [6] P. G. Kwiat, K. Mattle, H. Weinfurter, A. Zeilinger, A. V. Sergienko, and Y. Shih, *Phys. Rev. Lett.* **75**, 4337 (1995).
  - [7] C. Simon, M. Afzelius, J. Appel, A. Boyer de La Giroday, S. Dewhurst, N. Gisin, C. Hu, F. Jelezko, S. Kröll, J. Müller *et al.*, *Eur. Phys. J. D* **58**, 1 (2010).
  - [8] L. S. Madsen, F. Laudenbach, M. F. Askarani, F. Rortais, T. Vincent, J. F. Bulmer, F. M. Miatto, L. Neuhaus, L. G. Helt, M. J. Collins *et al.*, *Nature (London)* **606**, 75 (2022).
  - [9] B. Brecht, K.-H. Luo, H. Herrmann, and C. Silberhorn, *Appl. Phys. B* **122**, 116 (2016).
  - [10] Y. Jeronimo-Moreno, S. Rodriguez-Benavides, and A. B. U'Ren, *Laser Phys.* **20**, 1221 (2010).
  - [11] A. Moqanaki, F. Massa, and P. Walther, *APL Photon.* **4**, 090804 (2019).
  - [12] M. Scholz, F. Wolfgramm, U. Herzog, and O. Benson, *Appl. Phys. Lett.* **91**, 191104 (2007).
  - [13] U. Herzog, M. Scholz, and O. Benson, *Phys. Rev. A* **77**, 023826 (2008).
  - [14] K.-H. Luo, H. Herrmann, S. Krapick, B. Brecht, R. Ricken, V. Quiring, H. Suche, W. Sohler, and C. Silberhorn, *New J. Phys.* **17**, 073039 (2015).
  - [15] M. M. Fejer, G. Magel, D. H. Jundt, and R. L. Byer, *IEEE J. Quantum Electron.* **28**, 2631 (1992).
  - [16] A. Christ, A. Eckstein, P. J. Mosley, and C. Silberhorn, *Opt. Express* **17**, 3441 (2009).
  - [17] A. Gatti, T. Corti, and E. Brambilla, *Phys. Rev. A* **92**, 053809 (2015).
  - [18] A. Gatti and E. Brambilla, *Phys. Rev. A* **97**, 013838 (2018).
  - [19] C. Canalias and V. Pasiskevicius, *Nat. Photon.* **1**, 459 (2007).
  - [20] X. Xu, T. Wang, P. Chen, C. Zhou, J. Ma, D. Wei, H. Wang, B. Niu, X. Fang, D. Wu *et al.*, *Nature (London)* **609**, 496 (2022).
  - [21] Y.-C. Liu, D.-J. Guo, K.-Q. Ren, R. Yang, M. Shang, W. Zhou, X. Li, C.-W. Sun, P. Xu, Z. Xie *et al.*, *Sci. Rep.* **11**, 12628 (2021).
  - [22] R. Ikuta, R. Tani, M. Ishizaki, S. Miki, M. Yabuno, H. Terai, N. Imoto, and T. Yamamoto, *Phys. Rev. Lett.* **123**, 193603 (2019).
  - [23] M. Mehmet, S. Ast, T. Eberle, S. Steinlechner, H. Vahlbruch, and R. Schnabel, *Opt. Express* **19**, 25763 (2011).
  - [24] L. Gao, F. Lemarchand, and M. Lequime, *J. Eur. Opt. Soc.* **8** (2013).
  - [25] D. E. Zelmon, D. L. Small, and D. Jundt, *J. Opt. Soc. Am. B* **14**, 3319 (1997).
  - [26] S. Sarkar, V. Gupta, M. Kumar, J. Schubert, P. T. Probst, J. Joseph, and T. A. König, *ACS Appl. Mater. Interfaces* **11**, 13752 (2019).
  - [27] M. N. Polyanskiy, Refractive index database, <https://refractiveindex.info> (2023), accessed on 2023-05-10.
  - [28] Z. Yang, M. Liscidini, and J. E. Sipe, *Phys. Rev. A* **77**, 033808 (2008).
  - [29] M. Liscidini, L. Helt, and J. E. Sipe, *Phys. Rev. A* **85**, 013833 (2012).
  - [30] V. Introini, M. Steel, J. Sipe, L. Helt, and M. Liscidini, *Opt. Lett.* **45**, 1244 (2020).
  - [31] D. A. Roberts, *IEEE J. Quantum Electron.* **28**, 2057 (1992).
  - [32] M. Banic, L. Zatti, M. Liscidini, and J. E. Sipe, *Phys. Rev. A* **106**, 043707 (2022).
  - [33] O. Slattery, L. Ma, P. Kuo, and X. Tang, *Appl. Phys. B* **121**, 413 (2015).
  - [34] D. Rieländer, A. Lenhard, M. Mazzera, and H. De Riedmatten, *New J. Phys.* **18**, 123013 (2016).
  - [35] J. Eberly, *Laser Phys.* **16**, 921 (2006).
  - [36] P. Tapster and J. Rarity, *J. Mod. Opt.* **45**, 595 (1998).
  - [37] H. Takesue and K. Shimizu, *Opt. Commun.* **283**, 276 (2010).
  - [38] N. Ismail, C. C. Kores, D. Geskus, and M. Pollnau, *Opt. Express* **24**, 16366 (2016).